Available online at www.sciencedirect.com

ScienceDirect

Energy Procedia 155 (2018) 269–279

Energy Procedia

www.elsevier.com/locate/procedia

12th International Renewable Energy Storage Conference, IRES 2018

Synthetic strategies for the enhancement of $Mg(OH)_2$ thermochemical performances as heat storage material

Elpida Piperopoulos[a,b,*], Emanuela Mastronardo[a,b], Marianna Fazio[a], Maurizio Lanza[c], Signorino Galvagno[a], Candida Milone[a,b]

[a] *Department of Engineering, University of Messina, Contrada di Dio, 98166 Messina, Italy*
[b] *National Interuniversity Consortium of Materials Science and Technology (INSTM), 9 G. Giusti, 50121 Firenze, Italy*
[c] *Institute for Chemical and Physical Processes, National Research Council (CNR), 37 Ferdinando Stagno d'Alcontres, 98158 Messina, Italy*

Abstract

This work deals with the study of influence of multi walled carbon nanotubes (CNTs) characteristics on thermochemical performance of hybrid materials based on $Mg(OH)_2$ (M) as heat storage medium. Two different functionalized CNTs samples are investigated, separated curly tubes (SN) and bundles of straight nanotubes (BN). Hybrids were synthesized by reverse deposition precipitation method and their structure was characterized by X-ray analysis and scanning electron microscopy. The heat storage performance was studied through a thermogravimetric apparatus, simulating heat storage/release cycles. It is demonstrated that separated CNTs owning mainly carboxylic groups increase the interaction with precipitated magnesium hydroxide, improving the reacted fraction during dehydration/hydration cycle. In terms of dehydration/hydration conversion the samples' rank is SN-M>$Mg(OH)_2$>BN-M. SN-M exhibits higher heat storage/output capacity (~1250 kJ/$kg_{Mg(OH)2}$, ~350 MJ/m^3).

© 2018 The Authors. Published by Elsevier Ltd.
This is an open access article under the CC BY-NC-ND license (https://creativecommons.org/licenses/by-nc-nd/4.0/)
Selection and peer-review under responsibility of the scientific committee of the 12th International Renewable Energy Storage Conference.

Keywords: Thermochemical heat storage; $Mg(OH)_2$; Carbon nanotubes

1. Introduction

Systems are generally subjected to energy losses, which in most cases occur in the form of heat released to the environment. If stored, these waste heats can serve as an energetic resource for other processes inside or outside the system. Moreover, storing the excess of heat generated from solar power plants and re-use the stored heat when the

1876-6102 © 2018 The Authors. Published by Elsevier Ltd.
This is an open access article under the CC BY-NC-ND license (https://creativecommons.org/licenses/by-nc-nd/4.0/)
Selection and peer-review under responsibility of the scientific committee of the 12th International Renewable Energy Storage Conference.
10.1016/j.egypro.2018.11.051

renewable resource (i.e. sunlight) is not available is fundamental to make these systems reliable and steady energy sources. Thermal Energy Storage (TES) is possible through the use of reversible chemical reactions, which store energy in the chemical bonds and release it when required [1].

The use of the following reversible chemical reaction [2] at middle temperature (200-400 °C):

$$Mg(OH)_2\ (s) \leftrightarrow MgO\ (s) + H_2O\ (v) \qquad \Delta H^0 = \pm\ 1389\ kJ/kg_{Mg(OH)2}$$

for storing (endothermic $Mg(OH)_2$ dehydration reaction) and releasing heat on demand (exothermic MgO hydration) is still at an early stage development. Its actual limitation is the low thermal conductivity and poor durability of the storage medium to several dehydration/hydration reactions, decreasing its efficiency of ~50% after only three cycles. To overcome these drawbacks the use of a carbonaceous phase was used [3–7]. Literature studies demonstrated enhanced performances, in terms of heat stored capacity and durability, for CNTs/magnesium hydroxide hybrid materials [5]. In particular, almost all the theoretical heat storage capacity of Mg(OH)2 was exploited using functionalized CNTs [5]. But CNTs exist in several shapes [8]. In this study, it is investigated the influence of CNTs characteristics on thermochemical performance of hybrid materials. Two different functionalized CNTs samples were used, separated curly tubes [9] and bundles of straight nanotubes [10]. The heat storage performance was studied through a laboratory-scale simulation of the heat storage/release cycles.

Nomenclature

M	$Mg(OH)_2$
SN	separated curly tubes
BN	bundles of straight nanotubes
ΔH^0	standard enthalpy of $Mg(OH)_2$/MgO reaction (kJ mol^{-1})
m_{in}	initial sample mass (g)
m_{ist}	instantaneous mass (g)
$M_{Mg(OH)2}$	molecular weight of $Mg(OH)_2$ (g mol^{-1})
M_{MgO}	molecular weight of MgO (g mol^{-1})
$W_{Mg(OH)2}$	$Mg(OH)_2$ load (%)
Q_r	released heat per initial mass unit of $Mg(OH)_2$ (kJ $kg_{Mg(OH)2}^{-1}$)
Q_s	stored heat per initial mass unit of $Mg(OH)_2$ (kJ $kg_{Mg(OH)2}^{-1}$)
Q^M_r	released heat per mass unit (kJ $kg_{Mg(OH)2}^{-1}$)
Q^M_s	stored heat per mass unit (kJ $kg_{Mg(OH)2}^{-1}$)
Q^V_r	released heat per volume unit (MJ m^{-3})
Q^V_s	stored heat per volume unit (MJ m^{-3})
S_{BET}	specific surface area (m^2 g^{-1})
T_d	dehydration temperature (°C)
T_h	hydration temperature (°C)

Greek symbols

β	reacted fraction (%)
β^i_d	reacted fraction at the beginning of the dehydration treatment (%)
β^f_d	reacted fraction at the end of the dehydration treatment (%)
β_h	final reacted fraction of MgO at the point of water supply termination (%)
Δm_{real}	instantaneous real mass change (%)
Δm_{th}	theoretical mass change due to the dehydration of $Mg(OH)_2$ normalized to the total amount present in the sample (%)
$\Delta\beta_d$	dehydration conversion (%)
$\Delta\beta_h$	hydration conversion (%)
Δm	TG weight loss of carbon nanotubes (%)
ρ	apparent density of carbon nanotubes (kg m^{-3})

ρ_c	apparent density of the sample (kg m^{-3})

2. Experimental

2.1. Synthesis of CNTs and related CNTs based hybrid materials

CNTs were synthesized by Catalytic Chemical Vapor Deposition (CCVD). SN were synthesized by CCVD of iso-butane (i-C_4H_{10}) on Fe/Al_2O_3 catalyst, then purified to eliminate catalyst residue [9]. BN were synthesized by CCVD of methane (CH_4) on CoMoMg catalyst [10]. CNTs surface oxidation was carried out in nitric acid vapour (HNO_3) at T = 135 °C for 120 min, in agreement with the procedure reported elsewhere [11]. For the preparation of the hybrid materials a reverse deposition-precipitation method was employed [5]. Briefly, a specified amount of carbonaceous material (SN or BN) was sonicated for 30 min in 50 mL of $Mg(NO_3)_2$ (Sigma Aldrich, Saint Louis, USA, Assay: 99%) solution. Subsequently, 150 mL of NH_4OH 1 M (Carlo Erba, Milan, Italy, Assay: 30 wt %) solution was gradually added (2.5 mL/min) under magnetic stirring through a peristaltic pump. The final solution was aged at ambient conditions for 24 h, after which it was vacuum filtered (0.22 μm) and the collected solid was washed with deionized water and dried in a vacuum oven at 50 °C for 16 h. Pure $Mg(OH)_2$ was synthesized according to the precipitation reaction reported above.

2.2. Structural and morphological characterization of CNTs and hybrid materials

The morphology and crystal structure of the CNTs and hybrid materials obtained as described in §2.1 were studied by means of Scanning Electron Microscopy (SEM) - FEI Quanta 450 - and X-ray Diffraction (XRD) - Bruker D8 Advance - The SEM analysis were conducted on Cr metallized samples and operating with an accelerating voltage of 10/20 kV in high vacuum conditions). XRD patterns were collected by a Bragg-Brentano theta-2theta configuration, with Cu Kα radiation (40kV, 40 mA), in the range 10−80° with a step of 0.1°/s. Furthermore, to study any morphological and structural changes occurred, the samples were analysed after dehydration/hydration cyclic experiments.

2.3. Analysis of functional groups on CNTs surface

The number of oxygenated groups introduced upon oxidation was evaluated by means of Thermogravimetric Analysis (STA 449 F3 Jupiter, Netzsch, Selb, Germany). Samples were heated at 10 °C/min from 100 °C to 1000 °C using a constant flow rate of nitrogen (100 ml/min). Moreover, as heat-induced detachment of the various functional groups from the CNTs structure takes place in different temperature ranges, differential thermo-gravimetry (DTG) profiles provided information on their typology and relative amount [12].

The dispersibility of functionalized carbon nanotubes into 1M NH_4OH solution was investigated by measuring the sedimention time through Dynamic Light Scattering (DLS) analysis (Malvern Nano ZS ZEN3500).

2.4. Dehydration/Hydration cyclic experiments on hybrid materials

A thermogravimetric cycle for the investigation of the material's storage/release capacity consists of the completion of a dehydration and a hydration reaction. It was experimentally conducted by a TG unit (STA 449 F3 Jupiter, Netzsch, Selb, Germany) coupled with an evaporation system for the water vapour supply. A representative dehydration/hydration cycle was carried out on ~20 mg of sample as follows: first, the sample was dried at 110 °C in N_2 atmosphere (100 mL/min) for 60 min to desorb the physically-adsorbed water. Then, the temperature was increased at 10 °C/min to the dehydration temperature (T_d =350 °C) and kept for 120 min. Subsequently the temperature was decreased at −10 °C/min to the hydration temperature (T_h = 125 °C). The water vapour necessary for the MgO hydration reaction was supplied and mixed with N_2 as carrier gas, holding a partial pressure of 57.8 kPa. After 120 min, the water vapour supply was stopped, and the sample was kept at 110 °C for 10 min under 100 mL/min of N_2 atmosphere to physically remove the adsorbed water from the sample.

As reported elsewhere [6], the behaviour of the samples was expressed in terms of reacted fraction (β (%)), calculated by the Equation (1):

$$\beta\ (\%) = \left(1 - \frac{\Delta m_{real}}{\Delta m_{th}}\right) \times 100 \quad (1)$$

where Δm_{real} (%) is the instantaneous real mass change, and Δm_{th} (%) is the theoretical mass change due to the dehydration of 1 mol $Mg(OH)_2$ normalized to the total amount present in the sample, as expressed in Equations (2) and (3):

$$\Delta m_{real}(\%) = \left[\frac{(m_{in} - m_{inst})}{m_{in}}\right] \times 100 \quad (2)$$

$$\Delta m_{th}(\%) = \left[\frac{(M_{Mg(OH)_2} - M_{MgO})}{M_{Mg(OH)_2}}\right] \times W_{Mg(OH)_2} \quad (3)$$

where m_{in} (g) and m_{inst} (g) are respectively the initial sample mass and the instantaneous mass during the TG analysis. $M_{Mg(OH)2}$ (kg/mol) and M_{MgO} (g/mol) are, respectively, the molecular weight of $Mg(OH)_2$ and MgO, and $W_{Mg(OH)2}$ is the $Mg(OH)_2$ load. In the case of 100% weight of $Mg(OH)_2$ present in the sample Δm_{th}=30.89%.

The dehydration and hydration conversions ($\Delta\beta_{d/h}$ (%)) are respectively expressed by Equations (4) and (5):

$$\Delta\beta_d(\%) = \beta_d^i - \beta_d^f \quad (4)$$

$$\Delta\beta_h(\%) = \beta_h - \beta_d^f \quad (5)$$

where β^i_d (%) and β^f_d (%) are, respectively, the reacted fraction at the beginning and at the end of the dehydration treatment. While β_h (%) is the final reacted fraction of MgO at the point of water supply termination.

The heat storage and output capacities per mass ($Q^M_{s/r}$ ($kJ/kg_{Mg(OH)2}$)) and volume unit ($Q^V_{s/r}$ (MJ/m^3)) were calculated respectively by the following Equations (6) and (7):

$$Q^M_{s/r}(kJ/kg_{Mg(OH)_2}) = -\frac{\Delta H^0}{M_{Mg(OH)_2}} \times \frac{\Delta\beta_{d/h}}{100} \times 100 \quad (6)$$

$$Q^V_{s/r}(MJ/m^3) = -\frac{\Delta H^0}{M_{Mg(OH)_2}} \times \frac{\Delta\beta_{d/h}}{100} \times \rho_c \times \frac{W_{Mg(OH)_2}}{100} \quad (7)$$

where ΔH^0 (kJ/mol) is the enthalpy of reaction, and ρ_c (kg/m^3) is the density of the sample.

3. Results and Discussion

3.1. Comparison between the different CNTs used in hybrid materials' synthesis

Table 1 shows SN and BN properties.

Table 1. CNTs properties

Code	*Δm (%)*	*Δm (T=350 °C) (%)*	*ρ (kg/m³)*	*S_{BET} (m^2/g)*
SN	22.4	9.9	370	192.7
BN	28.3	9.7	400	138.5

Δm : TG weight loss at 1000 °C under inert atmosphere (N_2=100 ml/min), heating rate 10 °C/min

Δm (T=350 °C): TG weight loss at 350 °C under inert atmosphere (N_2=100 ml/min), heating rate 10 °C/min

S_{BET}: Specific surface area (BET calculation)

ρ: Apparent density

SN shows higher surface area and lower density. The quantity of oxygenated functionalities introduced upon oxidation with HNO_3 vapour is slightly higher for BN sample compared to SN (see Fig. 1a and Δm (%) in Table 1). DTG profiles (Fig. 1b) demonstrate that for BN, oxidation in HNO_3 vapours exhibits high selectivity toward the formation of carbonyl groups (-C=O) while for SN intensity signal is higher in the region of carboxylic acid groups (-COOH).

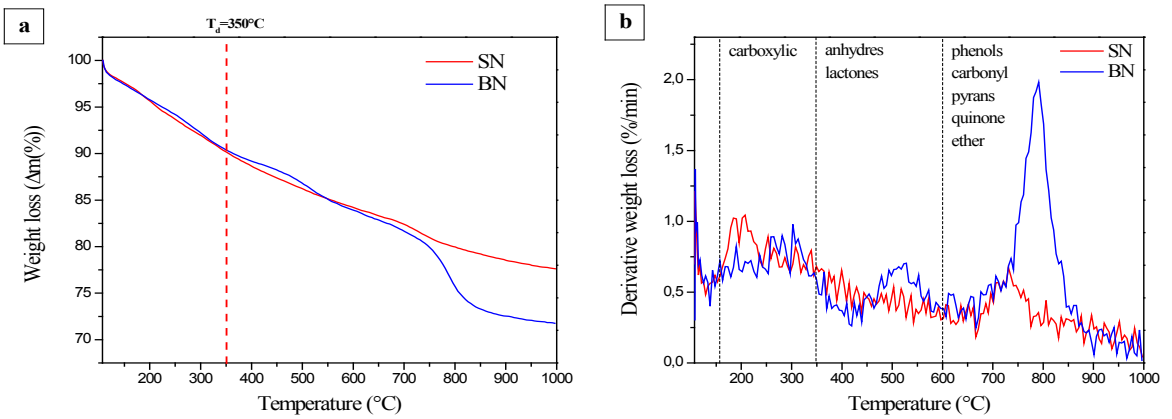

Fig. 1. (a) Thermogravimetric and (b) derivative thermogravimetric profiles of SN and BN in the temperature range between 100-1000 °C (heating rate: 10 °C/min) under inert atmosphere (N_2:100 ml/min).

SEM analysis reveals that the two samples present a completely different morphology. SN shows entanglements of curly tubes (Fig. 2a), whereas BN is mainly organized in bundles of straight CNTs (white circles in Fig.2b), forming a denser structure, as revealed by the higher apparent density reported in Table 1.

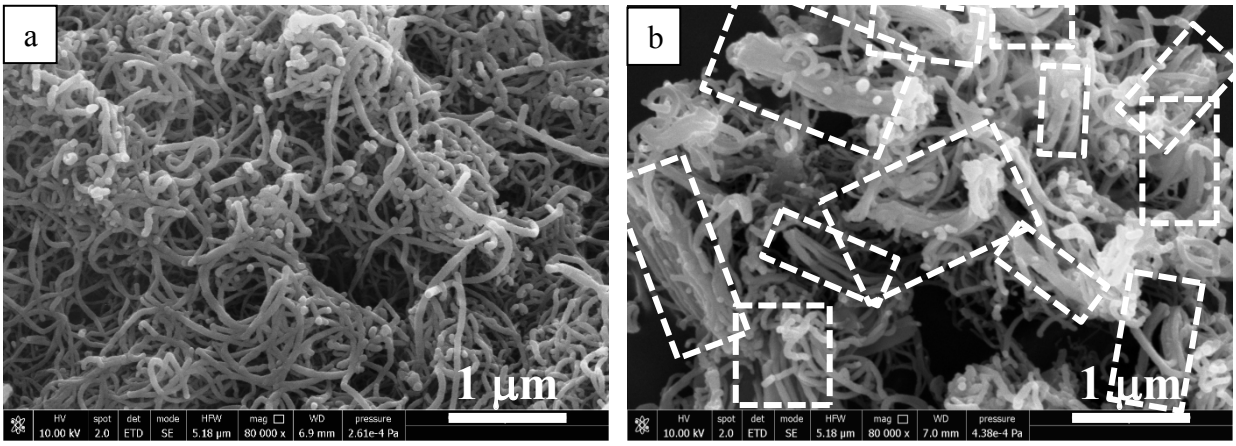

Fig. 2. SEM analysis of SN (a) and BN (b).

Fig. 3a shows the samples sedimentation at t=0 min, 30 min, 60 min and 24 h upon dispersion in 1M NH_4OH solution, that is the solution in which precipitation of $Mg(OH)_2$ occurs. The derived count rate (DCR – kcps in Fig. 3a) represents the light intensity detected by the DLS instrument, which is directly proportional to the sample concentration. Hence, the measure of the DCR at different times is indicative of the sample sedimentation rate. SN sample exhibits a constant DCR plot, meaning that no variation of concentration, thus no sedimentation occurs within the investigated time. On the contrary, BN sample shows a decreasing DCR plot that means sedimentation progressively occurs and completes after 24h. Photos in Fig. 3b clearly evidence the different dispersibility of investigated samples. This behaviour can be ascribed to the different polarity of CNTs surface. In particular SN sample, which contains the more polar carboxylic groups, presents an enhanced dispersibility into the polar medium [13] with respect to BN where the much less polar carbonyl groups are present (Fig. 1b). Moreover, it cannot be ruled out that the higher sedimentation rate of BN sample, composed by thicker bundles of straight CNTs, is due to the bigger aggregate's size. It is indeed know that the sedimentation rate is described by the Stokes' law, that at the same density of the material (see Table 1) and of the liquid solution and of the viscosity of the latter (NH_4OH 1M), it depends on the square of the dispersed particles' radius. Sayago et al. [14] reported that tightly packed Double walled NanoTubes self-organized in bundles hardly disperse with respect to untangled multi walled carbon nanotubes.

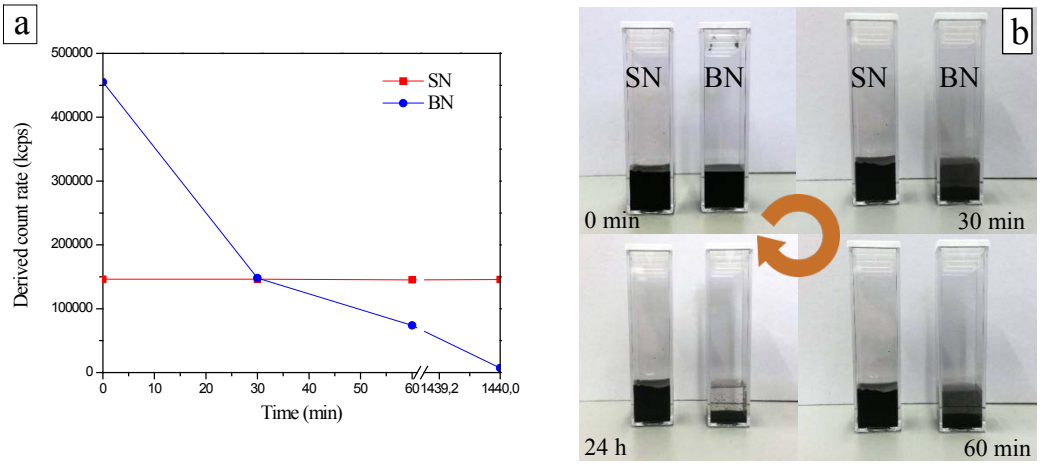

Fig. 3. a) DLS analysis on investigated CNTs; (b) Sedimentation test on SN (the left cuvette) and BN (the right cuvette)

3.2. Hybrid materials' morphological and structural characterization

The prepared hybrid materials are listed in Table 2, reporting the relative carbon type which the hybrid materials are made of, the $Mg(OH)_2$ load (wt. %), the bulk (or apparent) density and the surface area.

Table 2. CNTs based hybrid materials' properties

Code	$W_{Mg(OH)2}$ *(wt.%)*	*CNTs*	ρ_c *(kg/m³)*	S_{BET} *(m²/g)*
Mg(OH)₂	100.0	-	350	44.4
SN-M	36.4	SN	765	134.8
BN-M	43.0	BN	410	127.3

XRD analysis results (not shown for briefness) show in all the samples investigated, peaks relative to crystalline hexagonal brucite $Mg(OH)_2$ (2θ: 18.5°, 32.5°, 38°, 50.6°, 58.5°, 62°, 68°, 72°), accordingly with JCPDS 7-0239. In SN-M and BN-M also the carbonaceous phase is present (2θ: 26.5°, 42.5°, 45°, 51°, 55° in agreement with JCPDS 25-0284). No peaks arising from impurities are observed.

Hybrid materials show higher surface area in comparison with pure $Mg(OH)_2$ likely due to the contribution of CNTs. Despite the similar surface area, SN-M shows higher density (765 kg/m^3) than BN-M (410 kg/m^3), which is instead closer to that of pure $Mg(OH)_2$ (350 kg/m^3). These results can be explained at the light of the samples morphology. Indeed, from SEM analysis of fresh samples (Fig. 4.), it can be observed that in SN-M sample, $Mg(OH)_2$ particles are homogeneously dispersed into CNTs bundles thus allowing $Mg(OH)_2$ to occupy the voids of the open SN structure. Hence, a higher apparent density is measured. While, in BN-M, $Mg(OH)_2$ particles are densely agglomerated, forming compact layers covering the CNTs bundles thus limiting $Mg(OH)_2$ dispersion into the inner parts. So that predominantly, $Mg(OH)_2$ bulk density is measured. The different morphology of hybrid could be related with the different carbon phase dispersibility. In fact, stopping the magnetic stirring upon completing the addition of NH_4OH solution to $Mg(NO_3)_2$/CNTs suspensions, BN, settles more quickly in comparison with SN as reported in Fig. 3. Therefore it is likely that BN first sediments down at the bottom of the flask and $Mg(OH)_2$ forms a layer covering the entire structure of the carbonaceous material. Conversely due to the higher dispersibility, an homogeneous suspension containing SN and precipitated $Mg(OH)_2$ allows to achieve an intimate mixing between both phases. It should be also considered that the mixing between SN and $Mg(OH)_2$ can be promoted by the electrostatic interaction between carboxylic anion -COO^- and positively charged $Mg(OH)_2$ particles which forms at pH 11.5 [5].

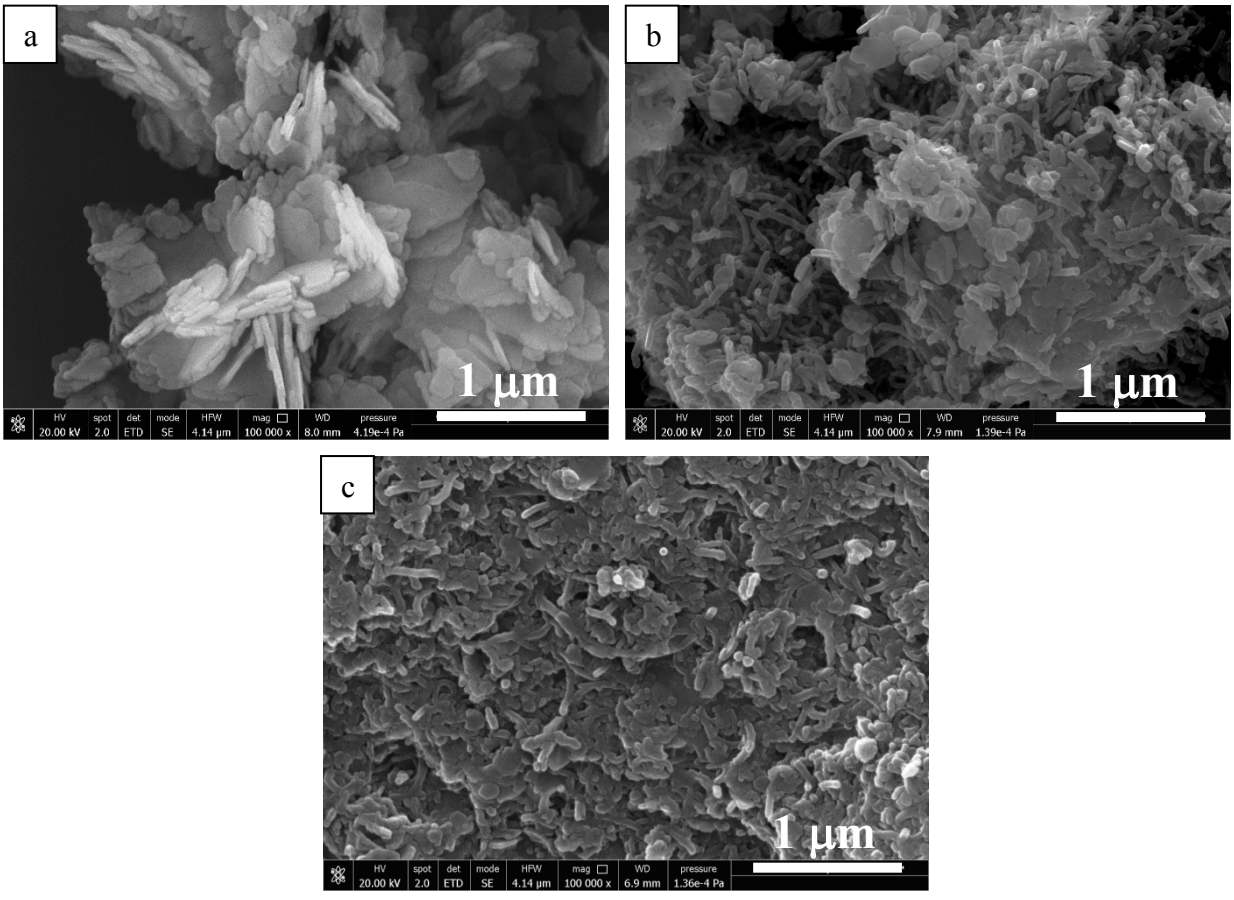

Fig. 4. SEM analysis of (a) $Mg(OH)_2$, (b) SN-M, (c) BN-M

3.3. Thermochemical behaviour

The hybrid samples, SN-M and BN-M, undergone to three dehydration/hydration cycles experiment under conditions reported in §2.3. For completeness, the samples were compared to pure $Mg(OH)_2$.

The curves plotted in Fig. 5. show the dehydration and hydration profiles, expressed as reacted fraction (β [%]) as a function of the reaction time (t [min]), relative to the third cycle, when the thermochemical behaviour of the samples was observed to be stable [4-7].

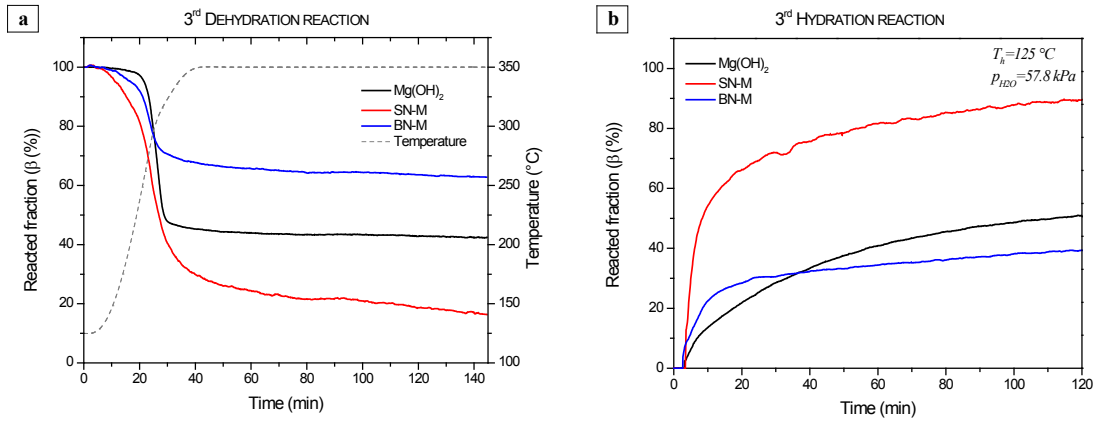

Fig.5. (a) Dehydration and (b) hydration curves relative to the 3rd cycle of pure $Mg(OH)_2$ (black curve), SN-M (red curve) and BN-M (blue curve).

It is evident from the dehydration profiles that pure $Mg(OH)_2$ undergoes to a separated decomposition step occurring between 200 °C and 350 °C (Fig. 5a black curve). SN-M and BN-M samples present a change in the curve slope, which is indicative of two overlapped processes taking place at different reaction rates (Fig. 5a red and blue curves). The fastest, which occurs between 200 °C and 350 °C, is clearly addressed to the $Mg(OH)_2$ dehydration reaction. The slowest, which occurs at lower temperatures (110–200 °C), is likely due to the structural water removal which can be retained by the hydrophilic oxygenated groups present on the carbonaceous surface [5]. Indeed, during the heating phase up to 350 °C to drive the $Mg(OH)_2$ dehydration, oxygenated groups present on SN and BN surfaces are only partially decomposed (see Fig. 1a). The remaining groups are able to physically retain the adsorbed water, thus explaining the first dehydration step even after three cycles [5].

In terms of dehydration/hydration conversion the samples' rank is SN-M>$Mg(OH)_2$>BN-M. Moreover, SN-M sample shows the highest hydration rate (Fig. 5b). These results can be clarified at the light of the samples morphology after three cycles experiments. From SEM images shown in Fig. 6., it is clear that in case of SN-M sample no significant changes can be observed with respect to as prepared sample (compare Fig. 4b and Fig. 6b). While, in case of pure $Mg(OH)_2$ and BN-M sample (Figs 4a,c and 6a,c), $Mg(OH)_2$ particles clearly coalesce, thus significantly limiting water vapour flow through the particles and MgO reconversion in $Mg(OH)_2$. This effect seems to be more pronounced in case of BN-M sample where a continuous and compact layer of active phase is formed thus further reducing the porosity of the material. As a result, the diffusion of water vapour is hindered inside particles thus only the surface layer reacts during the hydration step, reducing the material conversion.

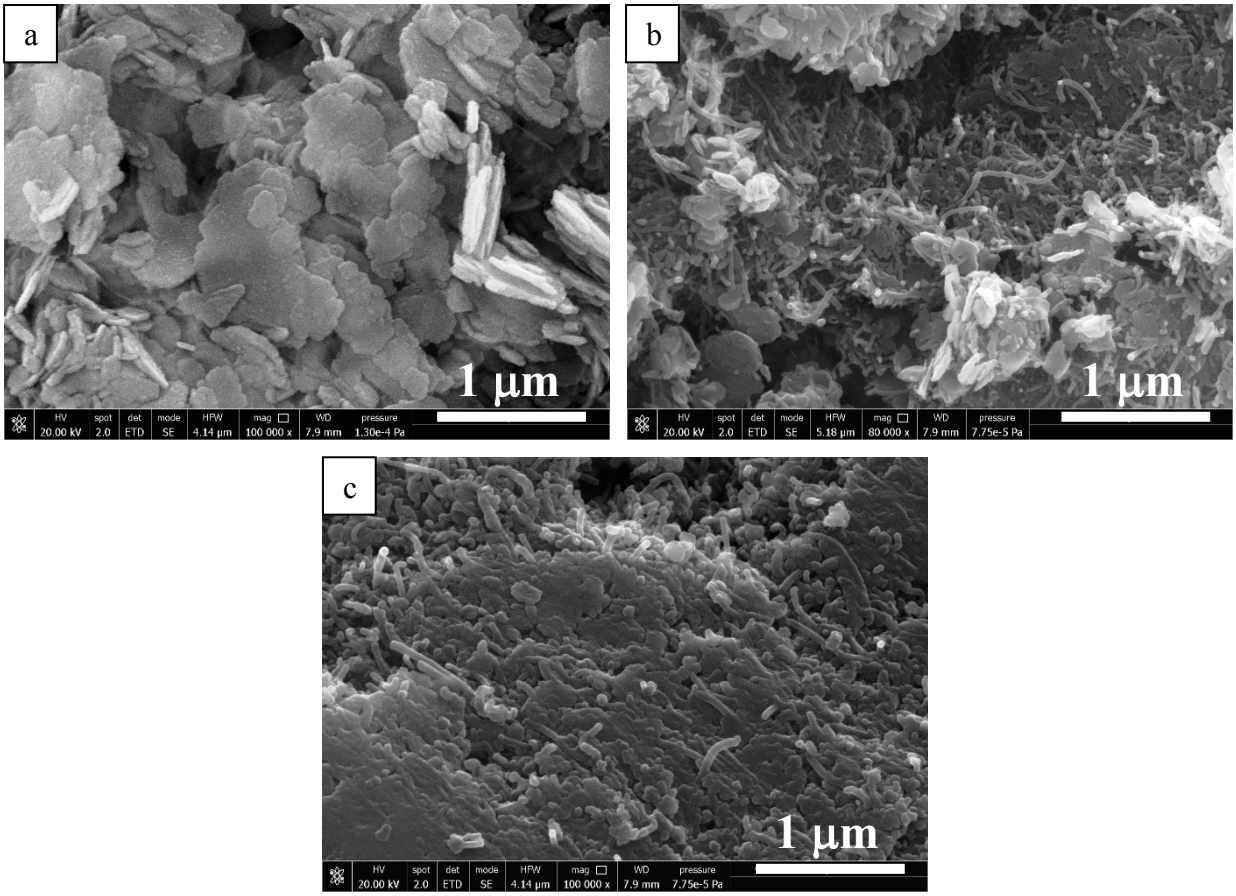

Fig. 6. SEM images of (a) pure $Mg(OH)_2$, (b) SN-M and (c) BN-M samples after three cycles experiments.

3.4. Heat storage and output capacities

The heat storage/output capacity per mass and volume unit of the investigated samples was evaluated through Equations 6 and 7, respectively. The curves of the cumulative stored/release heat as a function of time are reported in Fig. 7.

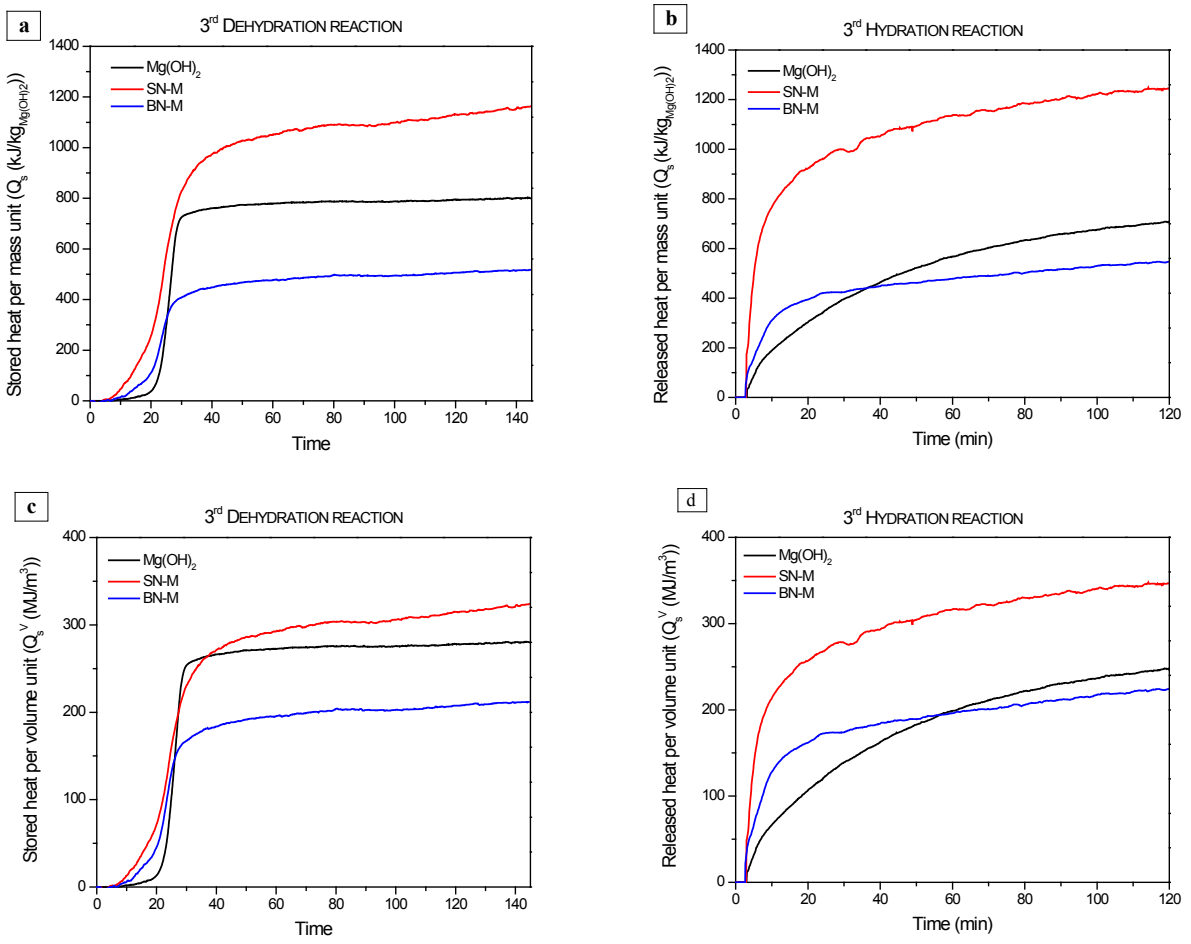

Fig. 7. Stored/released heat per (a, b) mass and (c, d) volume unit of pure $Mg(OH)_2$, SN-M and BN-M samples.

Whether in terms of mass or volume unit, SN-M exhibits higher heat storage/output capacity (~1250 kJ/$kg_{Mg(OH)2}$, ~350 MJ/m^3) with respect to pure $Mg(OH)_2$ (~700 kJ/$kg_{Mg(OH)2}$, ~250 MJ/m^3) and BN-M (~550 kJ/$kg_{Mg(OH)2}$, ~220 MJ/m^3). As it can be observed from the heat storage capacity curves (Figs 7a, c), pure $Mg(OH)_2$ shows a steeper slope and so a faster heat storage rate. On the contrary, from the slope of the heat output capacity curves (Figs 7b, d) it is evident that both SN-M and BN-M, due to their higher surface area, as reported in Table 2, are able to release the stored heat faster.

4. Conclusion

In this study functionalized CNTs-$Mg(OH)_2$ hybrid materials were investigated to study the influence of CNTs characteristics on thermochemical heat storage application. Two different CNTs were studied. SN sample shows entanglements of separated curly tubes, while BN is organized in bundles of straight CNTs. It is found that the use of SN or BN carbon nanotubes influences the morphology of final hybrid and then its thermochemical performance.

In SN-M sample, $Mg(OH)_2$ particles are homogeneously dispersed into CNTs thus allowing $Mg(OH)_2$ to occupy the voids of the open SN structure, while, in BN-M, $Mg(OH)_2$ particles are densely agglomerated, forming compact layer covering the CNTs. The latter morphology limits the conversion of active phase thus reducing the stored/released heat (~550 $kJ/kg_{Mg(OH)2}$, ~220 MJ/m^3), in comparison with SN-M (~1250 $kJ/kg_{Mg(OH)2}$, ~350 MJ/m^3) and pure $Mg(OH)_2$ (~700 $kJ/kg_{Mg(OH)2}$, ~250 MJ/m^3) samples.

References

[1] Sabihuddin, Siraj, Kiprakis, Aristides E., and Markus Mueller. "A numerical and graphical review of energy storage technologies." *Energies* 8(1) (2015): 172–216, doi:10.3390/en8010172.

[2] Kato, Yukitaka, Takahashi, Fu-uta, Watanabe, Akihiko, and Yoshio Yoshizawa. "Thermal analysis of a magnesium oxide/water chemical heat pump for cogeneration." *Appl. Therm. Eng.* 21(10) (2001): 1067–1081, doi:10.1016/S1359-4311(00)00103-4.

[3] Zamengo, Massimiliano, Ryu,Junichi, and Yukitaka Kato. "Magnesium hydroxide - Expanded graphite composite pellets for a packed bed reactor chemical heat pump." *Appl. Therm. Eng.* 61(2) (2013): 853–858, doi:10.1016/j.applthermaleng.2013.04.045.

[4] Mastronardo, Emanuela, Bonaccorsi, Lucio, Kato, Yukitaka, Piperopoulos, Elpida and Candida Milone. "Efficiency improvement of heat storage materials for $MgO/H_2O/Mg(OH)_2$ chemical heat pumps." *Appl. Energy* 162 (2016): 31–39, doi.org/10.1016/j.apenergy.2015.10.066.

[5] Mastronardo, Emanuela, Bonaccorsi, Lucio, Kato, Yukitaka, Piperopoulos, Elpida, Lanza, Maurizio and Candida Milone. "Thermochemical performance of carbon nanotubes based hybrid materials for $MgO/H_2O/Mg(OH)_2$ chemical heat pumps." *Appl. Energy* 181 (2016): 232–243, doi.org/10.1016/j.apenergy.2016.08.041.

[6] Mastronardo, Emanuela, Kato, Yukitaka, Bonaccorsi, Lucio, Piperopoulos, Elpida, and Candida Milone. "Thermochemical storage of middle temperature wasted heat by functionalized C/Mg(OH) hybrid materials." *Energies* 10 (1) (2017): 70-85, doi:10.3390/en10010070.

[7] Mastronardo, Emanuela, Bonaccorsi, Lucio, Kato, Yukitaka, Piperopoulos, Elpida, Lanza, Maurizio, and Candida Milone. "Strategies for the enhancement of heat storage materials performances for $MgO/H_2O/Mg(OH)_2$ thermochemical storage system." *Appl. Therm. Eng.* 120 (2017): 626–634, doi:10.1016/j.applthermaleng.2017.04.004.

[8] Zhang, Mei, and Jian Li. "Carbon nanotube in different shapes." *Mater. Today* 12(6) (2009): 12–18, doi:10.1016/S1369-7021(09)70176-2.

[9] Messina, Giacomo, Modafferi, V., Santangelo, Saveria, Tripodi, P, Donato, Maria Grazia, Lanza, Maurizio, Galvagno, Signorino, Milone, Candida, Piperopoulos, Elpida, and Alessandro Pistone. "Large-scale production of high-quality multi-walled carbon nanotubes: Role of precursor gas and of Fe-catalyst support." *Diam. Relat. Mater.* 17 (2008): 1482–1488, doi:10.1016/j.diamond.2008.01.060.

[10] Santangelo, Saveria, Piperopoulos, Elpida, Lanza, Maurizio, Mastronardo, Emanuela, and Candida Milone. "Synthesis of three-dimensional macro-porous networks of carbon nanotubes by chemical vapor deposition of methane on Co/Mo/Mg catalyst." *Appl. Catal. A Gen*. 505 (2015): 487–493, doi:10.1016/j.apcata.2015.05.022.

[11] Milone, Candida, Piperopoulos, Elpida, Ansari, Shabana, Faggio, Giuliana and Saveria Santangelo. "Highly Versatile and Efficient Process for CNT Oxidation in Vapor Phase by Means of $Mg(NO_3)_2$–HNO_3–H_2O Ternary Mixture." *Fullerenes, Nanotub. Carbon Nanostructures.* 23(1) (2015): 1–5, doi:10.1080/1536383X.2013.858132.

[12] Santangelo, Saveria, Piperopoulos, Elpida, Fazio, Enza, Faggio, Giuliana, Ansari, Shabana, Lanza, Maurizio, Neri, Fortunato, Messina, Giacomo, and Candida Milone. "A safer and flexible method for the oxygen functionalization of carbon nanotubes by nitric acid vapors." *Appl. Surf. Sci.* 303 (2014): 446–455, doi:10.1016/j.apsusc.2014.03.023.

[13] Huang, Chen-Chia, Li, Hong-Song, and Chien-Hung Chen. "Effect of surface acidic oxides of activated carbon on adsorption of ammonia." *J. Hazard. Mater*. 159 (2008): 523–527, doi:10.1016/j.jhazmat.2008.02.051.

[14] Sayago, Isabel, Santos, Hernan, Horrillo, Maria Carmen, Aleixandre, Manuel, Fernández, Marìa Jesus, Terrado, Eva, Tacchini, I, Aroz, R, Maser, Wolfang K, Benito, Ana M, Martínez, M.T, Gutiérrez, J, and Edgar Muñoz, "Carbon nanotube networks as gas sensors for NO_2 detection." *Talanta*. 77 (2008): 758–764, doi:10.1016/j.talanta.2008.07.025.